International Journal of STEM Education for Sustainibility, Vol.4, No.2, 2024, pp. 213-228
e-ISSN 2798-5091. DOI. 10.52889/ijses.v4i2.389

Understanding the Terminal Velocity of Particle Motion in Fluids at the Senior High School Level with Numerical Experiments

Submitted 17 March 2024 Revised 23 April 2024 Accepted 25 June 2024

Hilarius Donatus Hun[1*], Raden Manzilah Mubarokah Fahra[2], Bella Yunisah Putri[3], Yasrifa Fitri Aufia[4], Jubaedah Jubaedah[5]

[1,2,3,4,5]Physics Teaching Program, Faculty of Mathematics and Natural Sciences, Institut Teknologi Bandung, Bandung, Indonesia

Corresponding Email: *hilariushun@gmail.com

Abstrak

Students can understand the terminal velocity of solid particles by analyzing their free-fall motion in a fluid. We show it using a program designed by (Arbie et al., 2019)(Arbie et al., 2021). We use two parameters, namely the particle-fluid density ratio and the particle diameter, to determine their effect on terminal velocity. The experimental results show that the terminal velocity increases linearly with changes in the magnitude of the two parameters. Then, we also show the effect of the Reynolds number on the magnitude of the error value produced in the experiment.

Keywords: Terminal Velocity, Free-Fall motion, Particle-Fluid Density Ratio, Particle Diameter, Reynolds Number

INTRODUCTION

The dynamics of the free fall motion of solid particles in a fluid can be studied by analyzing the drag force experienced by the particles (Maxey, 2017; Liu & Yu, 2022). Particle diameter, fluid velocity, fluid density, and fluid viscosity affect the magnitude of the drag force. This can be expressed in the form ($F = f(d, u, \rho, \mu)$). From this relationship, a dimensionless quantity can be described, namely the drag coefficient (CF), the magnitude of which depends on a number called the Reynolds number (White, 2011; Ouchene et al., 2015). The Reynolds number describes the ratio of the fluid's inertia to its viscosity. The mathematical formulation of the Reynolds number is written in the form $Re = \rho_f uL/\mu_f$, where ρ_f is the fluid density, u is the velocity of the fluid, L is the channel width, and μ_f is the fluid's dynamic viscosity (White, 2011; Ershadnia et al., 2020). Additionally, the drag force is influenced by the adhesive forces between the fluid and the bounding walls (Vowinckel et al., 2019). Nevertheless, the drag force can be neglected for cases where the channel width to particle diameter ratio is greater than 15 (Dan et al., 2023).

When a single particle falls freely into a fluid, its initial velocity sharply increases due to the gravitational force acting upon it (Fornari et al., 2019). However, after a while, the particle's speed no longer increases. The particle moves at a constant speed. This speed is called terminal velocity (Kaiser et al., 2017). This condition is achieved when the gravitational force has been balanced with the buoyancy and fluid drag force so that the resultant force acting on the particle equals zero. Thus, according to Newton's 1st law, the particle will move in a straight line at a constant speed (Liu et al., 2016; Zhou et al., 2022). Each model formulates fluid drag forces with a form highly dependent on particle geometry (Bagheri & Bonadonna, 2016). The Stokes model is the most frequently used model to analyze the falling motion of solid particles in viscous fluids (Dey et al., 2019).

The Stokes model is used in high school and university viscosity experiments to study terminal velocity (Michna & Rogowski, 2022). However, the Stokes model is only precise with experimental results when the parameters have high viscosity, low Reynolds number, and slow particle fall velocity (Bergougnoux et al., 2014; Mirzaee et al., 2019). Furthermore, in the Stokes model, the frictional force between the fluid and the container walls is neglected, so the fluid is assumed to be in a huge container (Zhang & Mohseni, 2019; Chukwuneke et al., 2022). When the selection of the experimental set does not consider the above conditions, the experimental results obtained will differ significantly from the Stokes model predictions (Dioguardi et al., 2018; Wang et al., 2020; Rauter, 2021).

Many methods have been discovered to determine the terminal velocity of a solid object falling freely in a fluid. For instance, research conducted by (Putra, 2022; Fahrudin, 2022; Syifa et al., 2022; Setiawati & Yohanes, 2017) employed video tracker software to analyze videos of falling objects in fluids to determine terminal velocity. Meanwhile, (Ardiansyah, 2017; Lubis, 2018) utilized the falling ball method for this purpose. Additionally, (Romadhon et al., 2019; Budiyono et al., 2022) employed Arduino-based sensors. These experimental methods necessitate various specialized equipment, which must be prepared before conducting the experiments. Consequently, viscosity experiments to study terminal velocity cannot be carried out in schools that lack complete experimental equipment.

Numerical experiments are a solution for teachers to carry out experimental school activities. Teachers can use their or school-owned laptops (Chen et al., 2016). Various parameter variations can be easily simulated and then adjusted to the calculation results of the Stokes model. This trial and error process is challenging in laboratory experiments because of limited equipment and takes much time. However, with the help of a simulation program, this can be done quickly (Kantas et al., 2014). This can then increase teachers' knowledge about the best parameters that can be used to assemble viscosity experiments so that the results are not much different from the Stokes model calculations (Chau et al., 2023). These numerical experiments can help students build their physics knowledge through experiments (De Bézenac et al., 2019).

We use a program developed by (Arbie et al., 2019; Arbie et al., 2021) to demonstrate an alternative experimental method teachers can use to conduct viscosity experiments in schools. Here, we investigate the effect of the particle-fluid density ratio and particle diameter on the

International Journal of STEM Education for Sustainibility, Vol.4, No.2, 2024, pp. 213-228
e-ISSN 2798-5091. DOI. 10.52889/ijses.v4i2.389

magnitude of the particle terminal velocity. Next, we compare the obtained results with existing fluid theory and relevant research.

METHOD

This is a numerical experiment program in Figure 1 created by (Arbie et al., 2019)(Arbie et al., 2021). This program will stop automatically when the iteration process is complete.

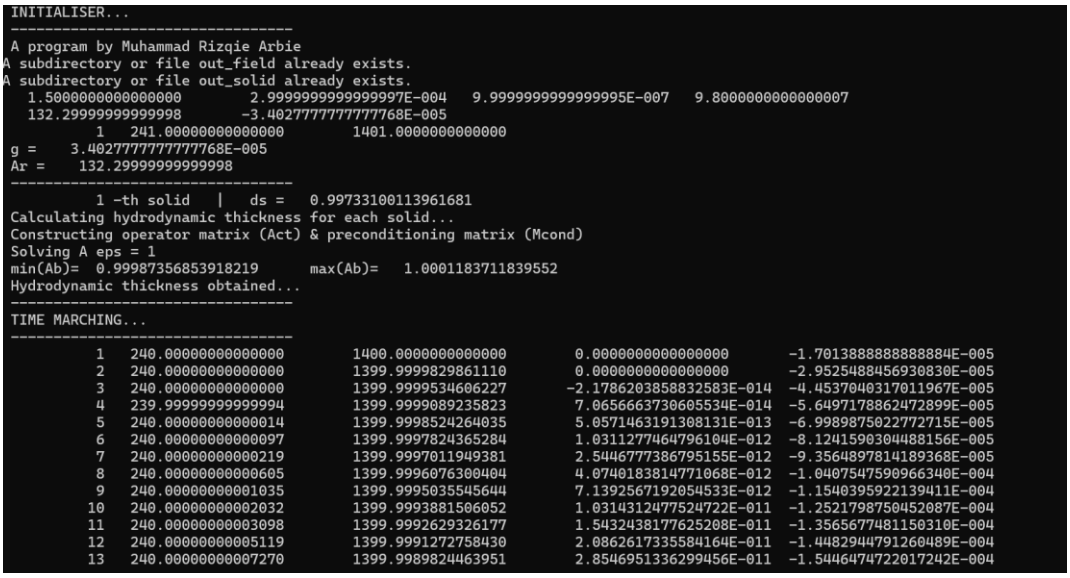

Figure 1. The interface of the program designed by (Arbie et al., 2019; Arbie et al., 2021)

The experimental program carried out was designed to accommodate two-dimensional particle configurations. It consists of two files, i.e., IBLBM_Ndisks_fast.exe, which functions as an executable to simulate the movement of particle in a viscous fluid, and parameters.dat, which contains the input parameters read by IBLBM_Ndisks_fast.exe. Figure 2 shows the parameters input into the notepad application. This input process is carried out before running the IBLBM_Ndisks_fast.exe program.

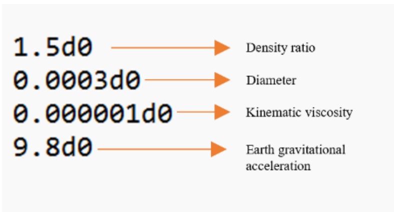

Figure 2. The parameters input into the notepad application

The experiment begins by inputting parameters such as density ratio, particle diameter, kinematic viscosity, and earth gravitational acceleration into the parameters.dat file. This file is then read in the Notepad application, and the input parameters are saved. Subsequently, the numerical experiment is initiated by executing the IBLBM_Ndisks_fast.exe file, a key component in the process. The choice of parameters is constrained by a dimensionless number called the Archimedes number, defined as;

International Journal of STEM Education for Sustainability, Vol.4, No.2, 2024, pp. 213-228
e-ISSN 2798-5091. DOI. 10.52889/ijses.v4i2.389

$$Ar = \left(\frac{\rho_s}{\rho_f} - 1\right)\frac{d^3 g}{v^2} \tag{1}$$

The selected parameters are set so that $Ar \leq 15000$. Figure 3 shows the output of IBLBM_Ndisks_fast.exe, i.e., fort 63 and fort 64. The terminal velocity component (v_y) data on the y-axis is used to analyze the terminal velocity of particles.

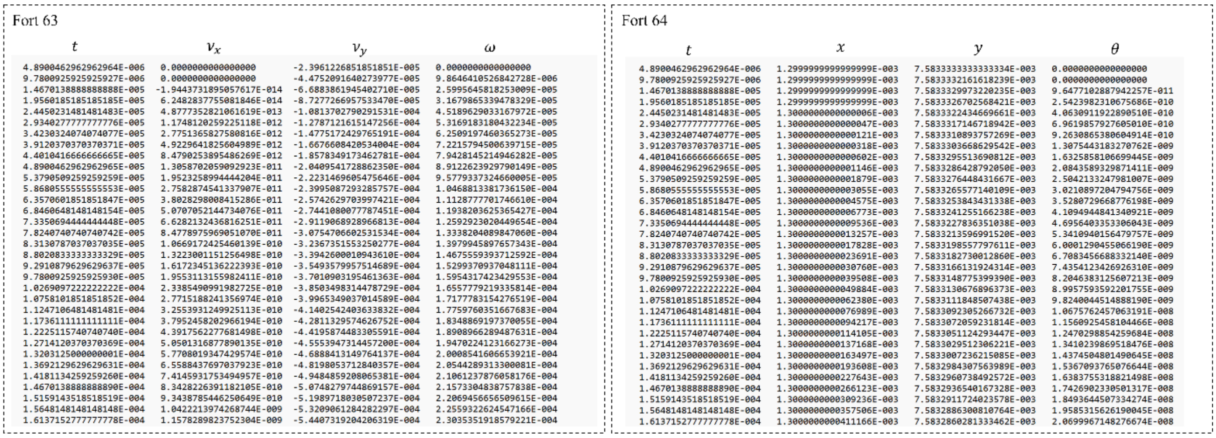

Fort 63

t	v_x	v_y	ω
4.8900462962962964E-006	0.0000000000000000	-2.3961226851851851E-005	0.0000000000000000
9.7800925925925927E-006	0.0000000000000000	-4.4752091640273977E-005	9.8646410526842728E-006
1.4670138888888888E-005	-1.9443731895057617E-014	-6.6883861945402710E-005	2.5995645818253009E-005
1.9560185185185185E-005	6.2482837755081846E-014	-8.7277266957533470E-005	3.1679865339478329E-005
2.4450231481481483E-005	4.8777352821061619E-013	-1.0813702790291531E-004	4.5189629033167972E-005
2.9340277777777776E-005	1.1748120259225118E-012	-1.2787121615147256E-004	5.3169183180432234E-005
3.4230324074074077E-005	2.7751365827580816E-012	-1.4775172429765191E-004	6.2509197460365273E-005
3.9120370370370371E-005	4.9229641825604989E-012	-1.6676608420534004E-004	7.2215794500639715E-005
4.4010416666666665E-005	8.4790253895486269E-012	-1.8578349173462781E-004	7.9428145214946282E-005
4.8900462962962965E-005	1.3058702059092923E-011	-2.0409541728862350E-004	8.9122623929790149E-005
5.3790509259259259E-005	1.9523258994444204E-011	-2.2231469605475646E-004	9.5779337324660005E-005
5.8680555555555553E-005	2.7582874541337907E-011	-2.3995087293285757E-004	1.0468813381736150E-004
6.3570601851851847E-005	3.8028298008415286E-011	-2.5742629703997421E-004	1.1128777701746610E-004
6.8460648148148154E-005	5.0707052144734076E-011	-2.7441080077787451E-004	1.1938203625365427E-004
7.3350694444444448E-005	6.6282132436816251E-011	-2.9119068928966813E-004	1.2592923020449654E-004
7.8240740740740742E-005	8.4778975969051070E-011	-3.0754706602531534E-004	1.3338204089847060E-004
8.3130787037037035E-005	1.0669172425460139E-010	-3.2367351553250277E-004	1.3979945897657343E-004
8.8020833333333329E-005	1.3223001151256498E-010	-3.3942600010943610E-004	1.4675559393712592E-004
9.2910879629629637E-005	1.6172345136222393E-010	-3.5493579957514689E-004	1.5299370937048111E-004
9.7800925925925930E-005	1.9553113155982411E-010	-3.7010903195461363E-004	1.5954317423429553E-004
1.0269097222222222E-004	2.3385490991982725E-010	-3.8503498314478729E-004	1.6557779219335814E-004
1.0758101851851852E-004	2.7715188241356974E-010	-3.9965349037014589E-004	1.7177783154276519E-004
1.1247106481481481E-004	3.2553931249925113E-010	-4.1402542403633832E-004	1.7759760351667683E-004
1.1736111111111111E-004	3.7952458202966194E-010	-4.2811329574626752E-004	1.8348869197370055E-004
1.2225115740740740E-004	4.3917562277681498E-010	-4.4195874483305591E-004	1.8908966289487631E-004
1.2714120370370369E-004	5.0501316877890135E-010	-4.5553947314457200E-004	1.9470224123166273E-004
1.3203125000000001E-004	5.7708019347429574E-010	-4.6888413149764137E-004	2.0008541606653921E-004
1.3692129629629631E-004	6.5588437697037923E-010	-4.8198053712840357E-004	2.0544289313300081E-004
1.4181134259259260E-004	7.4145931753494957E-010	-4.9484859208065381E-004	2.1061237876058176E-004
1.4670138888888890E-004	8.3428226391182105E-010	-5.0748279744869157E-004	2.1573304838757838E-004
1.5159143518518519E-004	9.3438785446250649E-010	-5.1989718030507237E-004	2.2069456656509615E-004
1.5648148148148148E-004	1.0422213974268744E-009	-5.3209061284282297E-004	2.2559322624547166E-004
1.6137152777777778E-004	1.1578289823752304E-009	-5.4407319204206319E-004	2.3035351918579221E-004

Fort 64

t	x	y	θ
4.8900462962962964E-006	1.2999999999999999E-003	7.5833333333333334E-003	0.0000000000000000
9.7800925925925927E-006	1.2999999999999999E-003	7.5833332161618239E-003	0.0000000000000000
1.4670138888888888E-005	1.2999999999999999E-003	7.5833329973220235E-003	9.6477102887942257E-011
1.9560185185185185E-005	1.2999999999999999E-003	7.5833326702568421E-003	2.5423982310675686E-010
2.4450231481481483E-005	1.3000000000000006E-003	7.5833322434669661E-003	4.0630911922890510E-010
2.9340277777777776E-005	1.3000000000000047E-003	7.5833317146718942E-003	6.9619857927605010E-010
3.4230324074074077E-005	1.3000000000000121E-003	7.5833310893757269E-003	9.2630865380604914E-010
3.9120370370370371E-005	1.3000000000000318E-003	7.5833303668629542E-003	1.3075443183270762E-009
4.4010416666666665E-005	1.3000000000000602E-003	7.5833295513690812E-003	1.6325858106699445E-009
4.8900462962962965E-005	1.3000000000001146E-003	7.5833286428792050E-003	2.0843589329871411E-009
5.3790509259259259E-005	1.3000000000001879E-003	7.5833276448431667E-003	2.5042133247981007E-009
5.8680555555555553E-005	1.3000000000003055E-003	7.5833265577140109E-003	3.0210897204794756E-009
6.3570601851851847E-005	1.3000000000004575E-003	7.5833253843431338E-003	3.5280729668776198E-009
6.8460648148148154E-005	1.3000000000006773E-003	7.5833241255166238E-003	4.1094944841340921E-009
7.3350694444444448E-005	1.3000000000009536E-003	7.5833227836351038E-003	4.6956403353306043E-009
7.8240740740740742E-005	1.3000000000013257E-003	7.5833213596991520E-003	5.3410940156479757E-009
8.3130787037037035E-005	1.3000000000017828E-003	7.5833198557797611E-003	6.0001290455066190E-009
8.8020833333333329E-005	1.3000000000023691E-003	7.5833182730012860E-003	6.7083456688332140E-009
9.2910879629629637E-005	1.3000000000030760E-003	7.5833166131924314E-003	7.4354123426926310E-009
9.7800925925925930E-005	1.3000000000039508E-003	7.5833148775399390E-003	8.2046383125607213E-009
1.0269097222222222E-004	1.3000000000049884E-003	7.5833130676896373E-003	8.9957593592201755E-009
1.0758101851851852E-004	1.3000000000062380E-003	7.5833111848507438E-003	9.8240044514888190E-009
1.1247106481481481E-004	1.3000000000076989E-003	7.5833092305266732E-003	1.0675762457063191E-008
1.1736111111111111E-004	1.3000000000094217E-003	7.5833072059231814E-003	1.1560925458104466E-008
1.2225115740740740E-004	1.3000000000114105E-003	7.5833051124293447E-003	1.2470298854259684E-008
1.2714120370370369E-004	1.3000000000137168E-003	7.5833029512306221E-003	1.3410239869518476E-008
1.3203125000000001E-004	1.3000000000163497E-003	7.5833007236215085E-003	1.4374504801490645E-008
1.3692129629629631E-004	1.3000000000193608E-003	7.5832984307563989E-003	1.5367093765076644E-008
1.4181134259259260E-004	1.3000000000227643E-003	7.5832960738492572E-003	1.6383755318821498E-008
1.4670138888888890E-004	1.3000000000266123E-003	7.5832936540167328E-003	1.7426902330501317E-008
1.5159143518518519E-004	1.3000000000309236E-003	7.5832911724023578E-003	1.8493644507334274E-008
1.5648148148148148E-004	1.3000000000357506E-003	7.5832886300810764E-003	1.9585315626190045E-008
1.6137152777777778E-004	1.3000000000411166E-003	7.5832860281333462E-003	2.0699967148276674E-008

Figure 3. The output of IBLBM_Ndisks_fast.exe, i.e., fort 63 and fort 64.

Experimental results are stored in files Fort 63 and Fort 64. Fort 63 contains time, linear velocity on the x and y axes, and angular velocity data. In contrast, Fort 64 contains the particles' time, horizontal and vertical position data, and angular position data. Subsequently, the terminal velocity component data on the y-axis is analyzed using Microsoft Excel to determine the terminal velocity of the particles. Figure 4 shows the forces acting on particles in a fluid

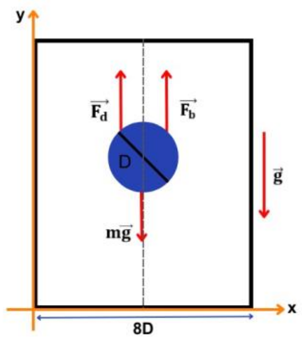

Figure 4. The forces acting on particles in a fluid

The terminal velocity obtained through numerical experiments is then compared with the analytical approach using Stokes' law for situations where particles are considered to have two dimensions. The condition of particles in the experiment is shown in Figure 1. particles falling in a fluid experience forces, as shown in Figure 1. Application of Newton's second law to particles produces:

$$mg - F_b - F_d = ma_y \tag{2}$$

In this study, particles are assumed to have a *2D* shape so that the Stokes drag force has the following form (Chen et al., 2021):

$$F_d = 4\pi k \mu_f U_s \tag{3}$$

Where is the Reynolds number corresponding to the *2D* particle shape as follows (Chen et al., 2021):

$$Re_p = \frac{d_p U_s}{v_f} \tag{4}$$

Equation (2) can be written as:

$$(\frac{\rho_p}{\rho_f} - 1)g - \frac{4kv_f}{r^2} U_s = \frac{\rho_p}{\rho_f}\frac{dU_s}{dt} \tag{5}$$

With $V_s = 4\pi r^2$ and $v_f = \frac{\mu_f}{\rho_f}$

Equation (5) is a first order ordinary linear differential equations. Solving the equation with the initial condition $U_s(0)$ = 0, produces:

$$U_s(t) = \left(\frac{\rho_s}{\rho_f} - 1\right)\frac{gr^2}{4kv_f}\left[1 - exp\left[-\frac{4kv_f}{\left(\frac{\rho_s}{\rho_f}\right)r^2}t\right]\right] \tag{6}$$

The terminal velocity is obtained When $t \to \infty$ so the shape becomes:

$$U_s = \left(\frac{\rho_s}{\rho_f} - 1\right)\frac{gr^2}{4kv_f} \tag{7}$$

The k value used has the following form(H. Chen et al., 2021):

$$k = \left(\ln \widehat{W} - 0{,}9157 + 1{,}722\widehat{W}^{-2} - 1{,}7302\widehat{W}^{-4} + 2{,}4056\widehat{W}^{-6} - 4{,}5913\widehat{W}^{-8}\right)^{-1}$$

Where $\widehat{W} = \frac{W}{d_s}$, in this experiment, the channel width (W) is set equal to $8d_s$ so that $\widehat{w}$=$\frac{W}{d_s} = 8$, So by plugging this result into equation (12), we get $k = 0{,}84$.

Table 1 shows the simulation parameters and their values applied in this study.

Table 1. Simulation parameters and their values applied in this study

Description	Symbol	Value	Unit
Particle-fluid density rasio	$\frac{\rho_s}{\rho_f}$	1,5-2,5	Dimensionless
Particle diameter	d_s	0,275-0,375	mm
Fluid kinematic viscosity	v_f	0,000001	m^2/s
Earth's gravitational acceleration	g	9,8	m/s^2
Correction factor	k	0,84	Dimensionless

To see how much the terminal velocity obtained analytically differs from the experiment, we use the percentage error expressed as follows:

$$\%\text{Error} = \left|\frac{U_{analytic} - U_{experiment}}{U_{experiment}} \times 100\%\right| \tag{8}$$

International Journal of STEM Education for Sustainibility, Vol.4, No.2, 2024, pp. 213-228
e-ISSN 2798-5091. DOI. 10.52889/ijses.v4i2.389

RESULTS AND DISCUSSION

In this numerical experiment, we chose water. In the first experiment, we varied the density ratio while keeping the particle diameter constant, and in the second experiment, we varied the particle diameter while keeping the density ratio constant as can be seen in Figure 5.

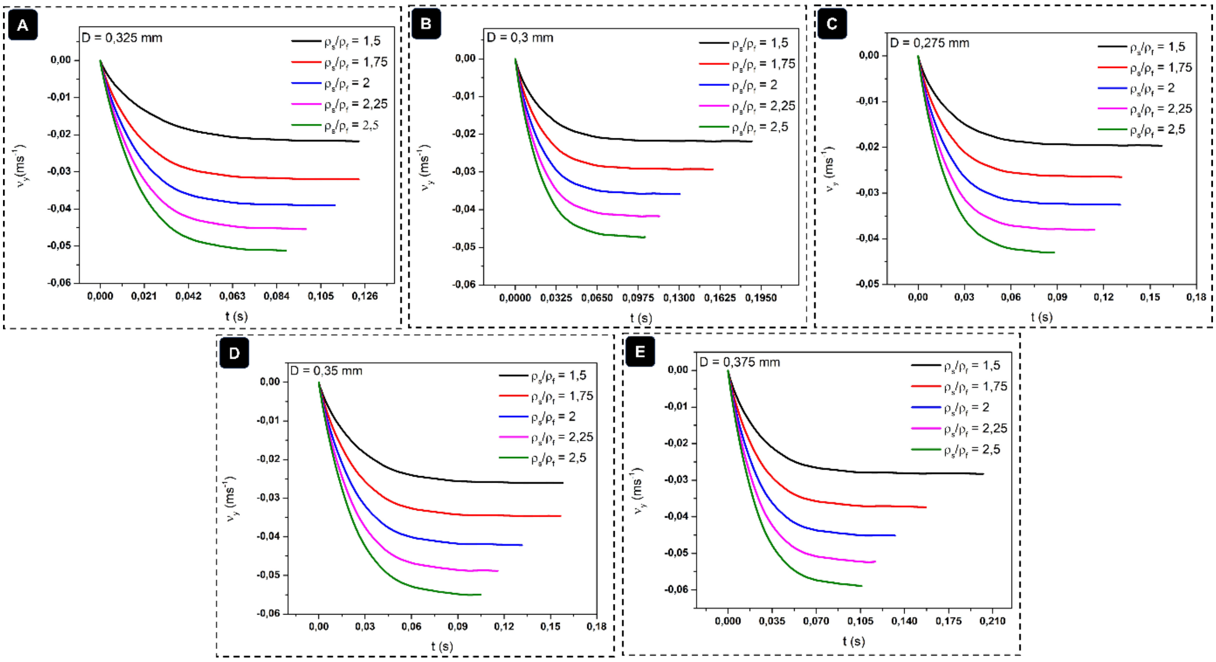

Figure 5. shows the results of the Fort 63 output. (a-e) terminal velocity graphs of particles with diameters of 0.275 mm, 0.3 mm, 0.325 mm, 0.35 mm, and 0.375 mm, respectively, with varying density ratios. Differences in density ratios cause variations in the terminal velocity curve. The greater the density ratio, the shorter the curve and the more it curves downward.

The results of the first experiment are shown in Figure 5. In each curve in Figure 5 (a-e), the curvature becomes sharper, and the curve length becomes shorter for higher density ratios. These observations can be explained qualitatively as follows.

Density ratio shows the ratio between particle density and fluid density. A density ratio greater than 1 indicates a stronger influence of gravitational force, while a ratio of 0 to 1 indicates a stronger influence of buoyancy (Shen et al., 2021). In our experiments, the density ratio used is greater than 1, indicating that the influence of gravitational force dominates. Consequently, for higher density ratios, the influence of gravitational force becomes more significant.

This significant influence causes the particle to accelerate at the onset of motion due to gravitational forces, which causes a steeper curvature in the terminal velocity curve for higher density ratios (Momenifar et al., 2019; Baker & Coletti, 2021). However, higher acceleration also causes the particle to experience a stronger drag force, causing the particle to reach terminal velocity more quickly. This effect shortens the terminal velocity curve to produce a higher density rasio (Wang et al., 2018; Shen et al., 2024). Table 2 shows the terminal velocity data with various density ratios obtained experimentally and analytically with appropriate errors and Reynolds number

Table 2. Terminal velocity data with various density ratios obtained experimentally and analytically with appropriate errors and Reynolds number

	$\frac{\rho_s}{\rho_f}$	Experiment (m/s)	Analytic (m/s)	% Error	Reynold Number
D = 0.275 mm	1,5	0,0196226571	0,027571615	40,51	5
	1,75	0,0264775326	0,041357422	56,20	7
	2	0,0325403796	0,055143229	69,46	9
	2,25	0,0380229985	0,068929036	81,28	10
	2,5	0,0430184674	0,082714844	92,28	12
D = 0.3 mm	1,5	0,0218544001	0,0328125	50,14	6
	1,75	0,0292948211	0,04921875	68,01	9
	2	0,0358623724	0,065625	82,99	11
	2,25	0,0417200202	0,08203125	96,62	12
	2,5	0,0472683157	0,0984375	108,25	14
D = 0.325 mm	1,5	0,0217691265	0,0385509115	76,90	7
	1,75	0,0320936902	0,057763672	79,98	10
	2	0,0389224256	0,077018229	97,88	13
	2,25	0,0454352932	0,096272786	111,89	15
	2,5	0,0512114176	0,115527344	125,59	17
D = 0.35 mm	1,5	0,0260517032	0,044661458	71,43	9
	1,75	0,03460913	0,066992188	93,57	12
	2	0,0421963473	0,089322817	111,68	15
	2,25	0,0488280036	0,0111653646	128,67	17
	2,5	0,0550237631	0,133984375	143,50	19
D = 0.375 mm	1,5	0,0282665184	0,051269531	81,38	11
	1,75	0,0373532881	0,076904297	105,88	14
	2	0,0451037934	0,102539063	127,34	17
	2,25	0,0524364928	0,128173828	144,43	20
	2,5	0,0588762461	0,153808584	161,24	22

It can be seen from Table 2 that the terminal velocity obtained from analytical calculations consistently exceeds the experimentally obtained terminal velocity. This disparity affects the magnitude of the error and the Reynolds number, with its value increasing with the density ratio (Li et al., 2022; Wang & Wang, 2022). We apply the Stokes model to compute the terminal velocity, where the Stokes drag force is a function of particulate velocity. However, in reality, the movement of particles in fluids is influenced by various interactions between particles, such as Van Der Waals forces, electrostatic forces, or liquid bridge forces. While the Stokes model provides an idealized representation of particle motion in fluids, it may not fully account for these additional factors. As a result, the terminal velocity calculated analytically tends to be higher due to the omission of these factors (Chen et al., 2021; Zhao et al., 2022; Wang et al., 2023). Figure 6 shows the results of the Fort 63 output. (a-e) terminal velocity graphs of particles with density ratio of 1.5, 1.75, 2, 2.25, and 2.5, respectively, with varying particle diameter. Differences in particle diameter cause variations in the terminal velocity curve. The greater the particle diameter, the shorter the curve and the more it curves downward.

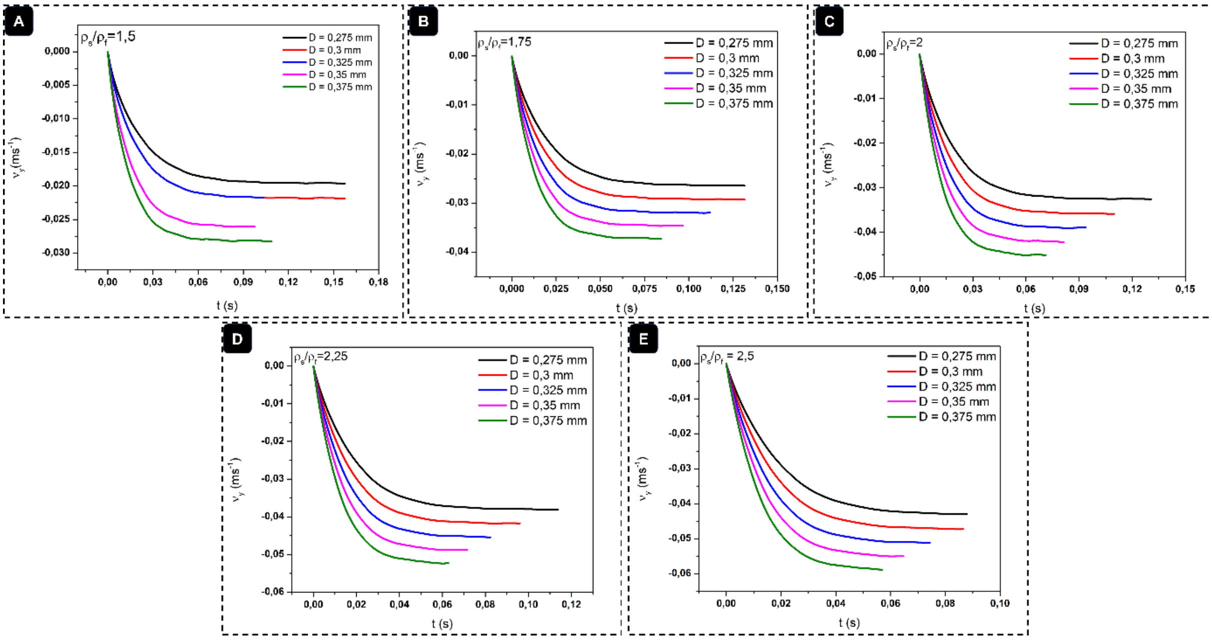

Figure 6. shows the results of the Fort 63 output. (a-e) terminal velocity graphs of particles with density ratio of 1.5, 1.75, 2, 2.25, and 2.5, respectively, with varying particle diameter. Differences in particle diameter cause variations in the terminal velocity curve.

The results of the second experiment are shown in Figure 6. Like the first experiment, each curve in Figure 6 (a-e) shows a sharper curvature as the input variable, particle diameter, increases. As previously explained, particle inertia significantly influences the initial motion of the particle. The magnitude of particle inertia is directly proportional to the diameter and acceleration of the particle. Consequently, particles with larger diameters exhibit curves with steeper slopes (Momenifar et al., 2019; Baker & Coletti, 2021).

Furthermore, as the particle moves faster due to its larger diameter, it experiences a more significant drag force, leading it to reach terminal velocity sooner. This phenomenon is evident in the curve corresponding to a particle diameter of 0.375 mm, which is shorter than curves associated with other diameters (Wang et al., 2018; Shen et al., 2024). Table 3 shows the terminal velocity data with various diameters obtained experimentally and analytically with appropriate errors and Reynolds number.

e-ISSN 2798-5091. DOI. 10.52889/ijses.v4i2.389

Table 3. Terminal velocity data with various diameters obtained experimentally and analytically with appropriate errors and Reynolds number

	D (mm)	Experiment (m/s)	Analytic (m/s)	% Error	Reynold Number
$\frac{\rho_s}{\rho_f}$ = 1.5	0.275	0.0196226571	0.027571615	40.51	5
	0.3	0.0218544001	0.0328125	50.14	6
	0.325	0.0217691265	0.0385509115	76.90	7
	0.35	0.0260517032	0.044661458	71.43	9
	0.375	0.0282665184	0.051269531	81.38	11
$\frac{\rho_s}{\rho_f}$ = 1.75	0.275	0.0264775326	0.041357422	56.20	7
	0.3	0.0292948211	0.04921875	68.01	9
	0.325	0.0320936902	0.057763672	79.98	10
	0.35	0.03460913	0.066992188	93.57	12
	0.375	0.0373532881	0.076904297	105.88	14
$\frac{\rho_s}{\rho_f}$ = 2	0.275	0.0325403796	0.055143229	69.46	9
	0.3	0.0358623724	0.065625	82.99	11
	0.325	0.0421963473	0.089322817	111.68	15
	0.35	0.0421963473	0.089322817	111.68	15
	0.375	0.0451037934	0.102539063	127.34	17
$\frac{\rho_s}{\rho_f}$ = 2.25	0.275	0.0380229985	0.068929036	81.28	10
	0.3	0.0417200202	0.08203125	96.62	12
	0.325	0.0454352932	0.096272786	111.89	15
	0.35	0.0488280036	0.0111653646	128.67	17
	0.375	0.0524364928	0.128173828	144.43	20
$\frac{\rho_s}{\rho_f}$ = 2.5	0.275	0.0430184674	0.082714844	92.28	12
	0.3	0.0472683157	0.0984375	108.25	14
	0.325	0.0512114176	0.115527344	125.59	17
	0.35	0.0550237631	0.133984375	143.50	19
	0.375	0.0588762461	0.153808584	161.24	22

It can be seen from Table 3 that the terminal velocity obtained from analytical calculations remains consistent with the findings presented in Table 2, being grater than the experimentally obtained terminal velocity. This trend also extends to errors and Reynolds numbers, with values increasing by the particle diameter (Li et al., 2022; Wang & Wang, 2022), as previously explained in Table 2.

The movement of particles in fluids is influenced by various factors, including interactions between particles such as Van Der Waals forces, electrostatic forces, or liquid bridging forces, which are not accounted for in the assumptions of the Stokes model. This omission results in the terminal velocity obtained from analytical calculations being more significant than that observed in experiments (Chen et al., 2021; Zhao et al., 2022; Wang et al., 2023).

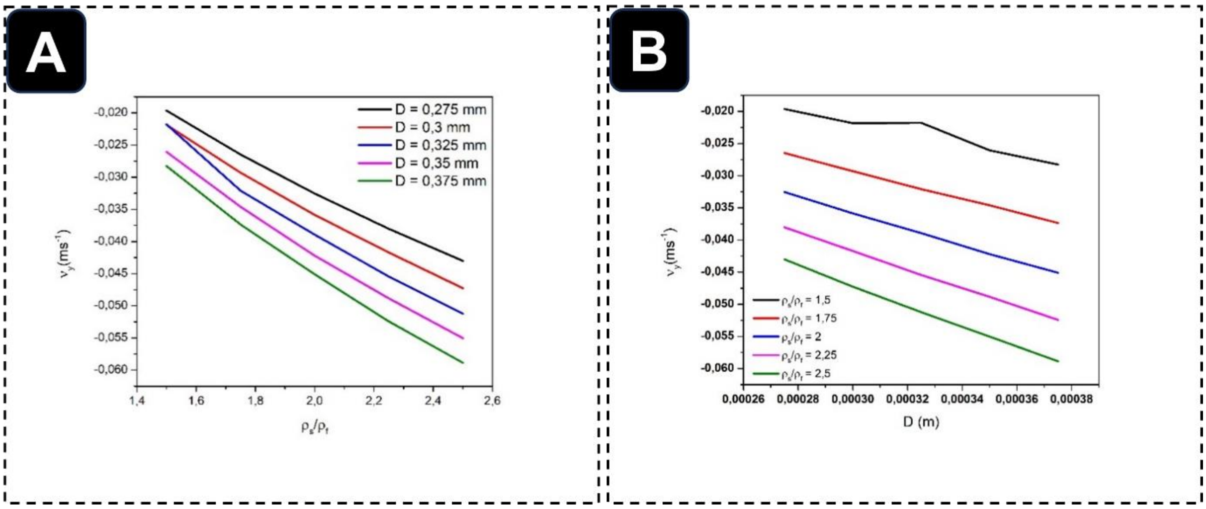

Subsequently, we attempted to compile terminal velocity data from the first and second experiments and plotted the resulting five graphs into one graph each. The outcomes are presented in Figures 7 and Figure 8, respectively.

8. The terminal velocity graphs from the second experiment.

It can be seen from Figure 7 dan Figure 8 that the terminal velocity of the particle is directly proportional to the ratio of its density and diameter. This relationship can be linked to equation (7), where the formulation of terminal velocity is proportional to the ratio of density and diameter of the particle. Previous studies conducted by (Rao et al., 2018) corroborate the findings in Figure 4a. Employing the same numerical method and particle shape, they observed that a higher density ratio corresponds to a faster attainment of terminal velocity, with the magnitude of terminal velocity proportional to the density ratio.

Figure 7. The terminal velocity graphs from the first experiment Figure

Furthermore, another previous study by (Lv et al., 2021) supports the results depicted in Figure 4b. They investigated the dynamics of kaolinite particle motion in water using the CFD-DEM simulation method. One of their research focuses on the accuracy of particle motion dynamics with models of non-spherical particles in fluids. Lv et al. (2021) reported that smaller particle diameters result in lower terminal velocities due to increased sensitivity to fluid resistance and water upwelling effects. In contrast, larger particle sizes indicate higher terminal velocities.

The results of data analysis from Tables 2 and 3 underscore the crucial role of the Reynolds number in fluid movement, as outlined by (White, 2011), The Reynolds numbers obtained, ranging from 0 to 100, signify a laminar fluid flow. This range is particularly significant as it demonstrates how the Reynolds number significantly influences fluid movement, a key finding in our research. The impact of the Reynolds number is vividly illustrated in Figure 9.

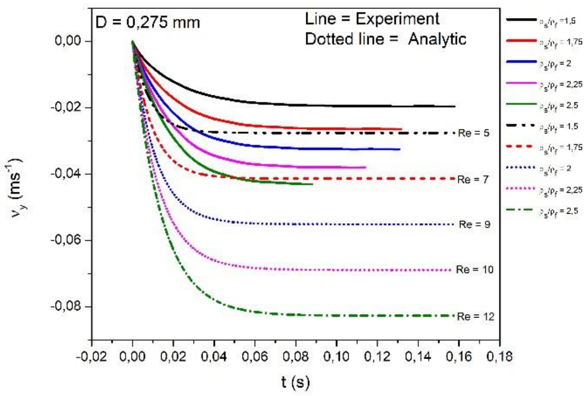

Figure 9. The terminal velocity curves obtained from experiments and analytical calculations.

Figure 9 further supports our findings, illustrating that at Reynolds numbers Re = 9, 10, and 12, significant differences in terminal velocities of particles between experimental and analytical results are observed. This significant difference shows that the Stokes model is only accurate at small Reynolds numbers. This is supported by the results obtained from (Shen et al., 2024), which state that at small Reynolds numbers, the Stokes drag force becomes the dominant force inhibiting particle motion. Therefore, at small Reynolds numbers, the terminal velocity obtained from the calculation approaches the experimental results. This is the knowledge that teachers need to conduct viscosity experiments. Teachers must arrange experimental sets so that they can produce small Reynolds numbers. This is done by choosing a viscous fluid with a smaller density ratio and particle diameter. In such circumstances, students can find a match between the Stokes model and their experimental results.

Similar findings were also reported by (Chen et al., 2021; Li et al., 2022) who conducted research using computational methods similar to those conducted by (Arbie et al., 2019; (Arbie et al., 2021; Chen et al., 2021) used water fluid with a channel width ratio to particle radius of 16. While (Li et al., 2022) conducted numerical experiments investigating the motion of kaolinite in fluids. They found differences in the terminal velocity obtained from experiments and analytical calculations as the Reynolds number increases.

CONCLUSION

The magnitude of the particle terminal velocity is proportional to the particle-fluid density ratio and particle diameter. The greater the value of the ratio of the fluid particle density and particle diameter, the more dominant the gravitational force becomes so that the particle velocity curve against time is steeper. This shows that the particles get greater acceleration. With the speed increasing faster and faster each time, the fluid drag force experienced by the particles is greater so that the particle speed reaches terminal velocity faster.

The increasing dominance of gravity in the fluid flow dynamics renders the analysis using the Stokes drag force inadequate. This is indicated by the Reynolds number, which increases proportionally with the two parameters. As the Reynolds number value increases, the discrepancy between the terminal velocity calculated using the Stokes model and the experimental results becomes more pronounced, highlighting the limitations of the Stokes model in these conditions.

These results are essential for teachers when designing viscosity practicums. Selecting the practicum set is easy if the practicum aims to see the relationship between particle-fluid density ratio and particle diameter with terminal velocity. However, if the practicum also directs students to predict the results using the Stokes model, selecting the practicum set must be more careful.

ACKNOWLEDGEMENT

H.D.H. and Y.F.A gratefully acknowledge the Indonesian Endowment Fund for Education (LPDP) for master scholarships. B.Y.P gratefully acknowledges Beasiswa Unggulan for master scholarships.

REFERENCES

Arbie, M. R., Fauzi, U., & Latief, F. D. (2019). Dynamics of two disks in a counter-flow using Immersed Boundary-Lattice Boltzmann method. *Computers & Fluids*, *179*, 265-276.

Arbie, M. R., Fauzi, U., Latief, F. D. E., & Mustopa, E. J. (2021). Two-Solid Deposition in Fluid Column using Immersed Boundary-Lattice Boltzmann Method. *Journal of Applied and Computational Mechanics*, *7*(3), 1814–1825. https://doi.org/10.22055/jacm.2021.37140.2969

Ardiansyah, D. (2017). PERANCANGAN DAN PENERAPAN SENSOR KUMPARAN UNTUK PERCOBAAN VISKOSITAS DENGAN METODE BOLA JATUH. *Jurnal Inovasi Fisika Indonesia*, *06*(01), 5–9.

Bagheri, G., & Bonadonna, C. (2016). On the drag of freely falling non-spherical particles. *Powder Technology*, *301*, 526–544. https://doi.org/10.1016/j.powtec.2016.06.015

Baker, L. J., & Coletti, F. (2021). Particle–fluid–wall interaction of inertial spherical particles in a turbulent boundary layer. *Journal of Fluid Mechanics*, *908*, A39. https://doi.org/10.1017/jfm.2020.934

Bergougnoux, L., Bouchet, G., Lopez, D., & Guazzelli, É. (2014). The motion of solid spherical particles falling in a cellular flow field at low Stokes number. *Physics of Fluids*, *26*(9). https://doi.org/10.1063/1.4895736

Budiyono, B., Sutrisno, E., & Wibowo, T. U. (2022). Design of a Falling Ball Speed Measuring Instrument in Viscosity Experiment Using Arduino UNO ATmega. *BERKALA SAINSTEK*, *10*(1), 10. https://doi.org/10.19184/bst.v10i1.27315

Chau, T., Ghazali, I., Nguyen, H., Nguyen, D., Ly, H., & Nguyen, T. (2023). A low-cost pitot tube-based experimental model for active teaching-learning of applied fluid mechanics: A demonstration from NTTU. *Engineering Science Letter*, *2*(03), 84–91. https://doi.org/10.56741/esl.v2i03.432

Chen, D. L., Schonger, M., & Wickens, C. (2016). oTree—An open-source platform for laboratory, online, and field experiments. *Journal of Behavioral and Experimental Finance*, *9*, 88–97. https://doi.org/10.1016/j.jbef.2015.12.001

Chen, H., Liu, W., Chen, Z., & Zheng, Z. (2021). A numerical study on the sedimentation of adhesive particles in viscous fluids using LBM-LES-DEM. *Powder Technology*, *391*, 467–478. https://doi.org/10.1016/j.powtec.2021.06.031

Chukwuneke, J. L., Aniemene, C. P., Okolie, P. C., Obele, C. M., & Chukwuma, E. C. (2022). Analysis of the Dynamics of a Freely Falling Body in a Viscous Fluid: Computational Fluid Dynamics Approach. *International Journal of Thermofluids*, *14*. https://doi.org/10.1016/j.ijft.2022.100157

Dan, P., Miao, L., Linfang, S., Zhiliang, W., & Zhenquan, L. (2023). The effects of channel width on particle sedimentation in fluids using a coupled lattice Boltzmann-discrete element model. *Physics of Fluids*, *35*(5). https://doi.org/10.1063/5.0147826

De Bézenac, E., Pajot, A., & Gallinari, P. (2019). Deep learning for physical processes: incorporating prior scientific knowledge. *Journal of Statistical Mechanics: Theory and Experiment*, *2019*(12), 124009. https://doi.org/10.1088/1742-5468/ab3195

Dey, S., Zeeshan Ali, S., & Padhi, E. (2019). Terminal fall velocity: the legacy of Stokes from the perspective of fluvial hydraulics. *Proceedings of the Royal Society A: Mathematical, Physical and Engineering Sciences*, *475*(2228), 20190277. https://doi.org/10.1098/rspa.2019.0277

Dioguardi, M., Di Gioia, G., Illuzzi, G., Laneve, E., Cocco, A., & Troiano, G. (2018). Endodontic irrigants: Different methods to improve efficacy and related problems. *European journal of dentistry*, *12*(03), 459-466.

Ershadnia, R., Amooie, M. A., Shams, R., Hajirezaie, S., Liu, Y., Jamshidi, S., & Soltanian, M. R. (2020). Non-Newtonian fluid flow dynamics in rotating annular media: Physics-based and data-driven modeling. *Journal of Petroleum Science and Engineering*, *185*, 106641. https://doi.org/10.1016/j.petrol.2019.106641

Fahrudin, A. (2022). Pengaruh Penggunaan Software Treker Terhadap Hasil Belajar Fisika Mahasiswa Pada Pokok Bahasan Viskositas Fluida. *Jurnal Pendidikan Sains Dan Komputer*, *2*(01), 41–48. https://doi.org/10.47709/jpsk.v2i01.1357

Fornari, W., Zade, S., Brandt, L., & Picano, F. (2019). Settling of finite-size particles in turbulence at different volume fractions. *Acta Mechanica*, *230*(2), 413–430. https://doi.org/10.1007/s00707-018-2269-1

Kaiser, D., Kowalski, N., & Waniek, J. J. (2017). Effects of biofouling on the sinking behavior of microplastics. *Environmental Research Letters*, *12*(12), 124003. https://doi.org/10.1088/1748-9326/aa8e8b

Kantas, N., Beskos, A., & Jasra, A. (2014). Sequential Monte Carlo Methods for High-Dimensional Inverse Problems: A Case Study for the Navier--Stokes Equations. *SIAM/ASA Journal on Uncertainty Quantification*, *2*(1), 464–489. https://doi.org/10.1137/130930364

Li, X., Liu, G., Zhao, J., Yin, X., & Lu, H. (2022). IBM-LBM-DEM Study of Two-Particle Sedimentation: Drafting-Kissing-Tumbling and Effects of Particle Reynolds Number and Initial Positions of Particles. *Energies*, *15*(9), 3297. https://doi.org/10.3390/en15093297

Liu, L., Yan, H., Zhao, G., & Zhuang, J. (2016). Experimental studies on the terminal velocity of air bubbles in water and glycerol aqueous solution. *Experimental Thermal and Fluid Science*, *78*, 254–265. https://doi.org/10.1016/j.expthermflusci.2016.06.011

Liu, Y., & Yu, X. (2022). General formulation of drag force on assemblage of spherical particles in fluids: A critical review and a new empirical formula. *Physics of Fluids*, *34*(6). https://doi.org/10.1063/5.0096069

Lubis, N. (2018). *PENGARUH KEKENTALAN CAIRAN TERHADAP WAKTU JATUH BENDA MENGGUNAKAN FALLING BALL METHOD THE INFLUENCE OF LIQUID VISCOSITY ON FALLING TIME BY FALLING BALL METHOD*. *2*(2), 26–32.

Lv, K., Min, F., Zhu, J., Ren, B., Bai, X., & Wang, C. (2021). Experiments and CFD-DEM simulations of fine kaolinite particle sedimentation dynamic characteristics in a water environment. *Powder Technology*, *382*, 60–69. https://doi.org/10.1016/j.powtec.2020.12.057

Maxey, M. (2017). Simulation Methods for Particulate Flows and Concentrated Suspensions. *Annual Review of Fluid Mechanics*, *49*(1), 171–193. https://doi.org/10.1146/annurev-fluid-122414-034408

Michna, J., & Rogowski, K. (2022). Numerical Study of the Effect of the Reynolds Number and the Turbulence Intensity on the Performance of the NACA 0018 Airfoil at the Low Reynolds Number Regime. *Processes*, *10*(5), 1004. https://doi.org/10.3390/pr10051004

Mirzaee, H., Rafee, R., & Ahmadi, G. (2019). Inertial impaction of particles on a circular cylinder for a wide range of Reynolds and P numbers: A comparative study. *Journal of Aerosol Science*, *135*, 86–102. https://doi.org/10.1016/j.jaerosci.2019.06.001

Momenifar, M., Dhariwal, R., & Bragg, A. D. (2019). Influence of Reynolds number on the motion of settling, bidisperse inertial particles in turbulence. *Physical Review Fluids*, *4*(5), 054301. https://doi.org/10.1103/PhysRevFluids.4.054301

Ouchene, R., Khalij, M., Tanière, A., & Arcen, B. (2015). Drag, lift and torque coefficients for ellipsoidal particles: From low to moderate particle Reynolds numbers. *Computers and Fluids*, *113*, 53–64. https://doi.org/10.1016/j.compfluid.2014.12.005

Putra, B. E. (2022). The IMPLEMENTATION OF PHYSICS LEARNING MEDIA IN VISCOSITY TUBE WITH VIDEO ANALYSIS USING SOFTWARE TRACKER. *Jurnal Pendidikan Fisika Dan Sains (JPFS)*, *5*(1), 10–15. https://doi.org/10.52188/jpfs.v5i1.207

Rao, Y., Liu, C., Wang, H., Ni, Y., Lv, C., Liu, S., Lan, Y., & Wang, S. (2018). Density ratio effect on particle sedimentation in a vertical channel. *Chinese Journal of Physics*, *56*(4), 1427–1438. https://doi.org/10.1016/j.cjph.2018.06.007

Rauter, M. (2021). The compressible granular collapse in a fluid as a continuum: validity of a Navier–Stokes model with , -rheology. *Journal of Fluid Mechanics*, *915*, A87. https://doi.org/10.1017/jfm.2021.107

Romadhon, N., Pratiwi, U., & Al Hakim, Y. (2019). KEEFEKTIFAN ALAT PERAGA VISKOSITAS DENGAN SENSOR MINI REED SWITCH MAGNETIC BERBASIS ARDUINO UNTUK MENINGKATKAN KEMAMPUAN ANALYZEPESERTA DIDIK. *Muslim Heritage*, *4*(2). https://doi.org/10.21154/muslimheritage.v4i2.1765

Setiawati, D., & Yohanes, R. (2017). Analisis Hubungan Kecepatan Terminal dengan Viskositas Zat Cair Menggunakan Software Tracker. *Jurnal Materi Dan Pembelajaran Fisika*, *17*, 1–6. https://doi.org/https://doi.org/10.20961/jmpf.v7i2.31378

Shen, J., Lu, Z., Wang, L.-P., & Peng, C. (2021). Influence of particle-fluid density ratio on the dynamics of finite-size particles in homogeneous isotropic turbulent flows. *Physical Review E*, *104*(2), 025109. https://doi.org/10.1103/PhysRevE.104.025109

Shen, J., Peng, C., Lu, Z., & Wang, L. P. (2024). The influence of particle density and diameter on the interactions between the finite-size particles and the turbulent channel flow. *International Journal of Multiphase Flow*, *170*. https://doi.org/10.1016/j.ijmultiphaseflow.2023.104659

Syifa, N. H., Hartono, H., & Sulhadi, S. (2022). DETERMINATION OF TERMINAL VELOCITY AND FLUID VISCOSITY USING FALLING BALL VISCOMETER WITH VIDEO TRACKER APLICATION. *JPF (Jurnal Pendidikan Fisika) Universitas Islam Negeri Alauddin Makassar*, *10*(2), 75–80. https://doi.org/10.24252/jpf.v10i2.22242

Vowinckel, B., Withers, J., Luzzatto-Fegiz, P., & Meiburg, E. (2019). Settling of cohesive sediment: particle-resolved simulations. *Journal of Fluid Mechanics*, *858*, 5–44. https://doi.org/10.1017/jfm.2018.757

Wang, D., Qian, Q., Zhong, A., Lu, M., & Zhang, Z. (2023). Numerical modeling of micro-particle migration in channels. *Advances in Geo-Energy Research*, *10*(2), 117–132. https://doi.org/10.46690/ager.2023.11.06

Wang, D., & Wang, Z. (2022). 3D Lattice Boltzmann Method-Discrete-Element Method with Immersed Moving Boundary Scheme Numerical Modeling of Microparticles Migration Carried by a Fluid in Fracture. *SPE Journal*, *27*(05), 2841–2862. https://doi.org/10.2118/209822-PA

Wang, L., Zheng, K., Ding, Z., Yan, X., Zhang, H., Cao, Y., & Guo, C. (2020). Drag coefficient and settling velocity of fine particles with varying surface wettability. *Powder Technology, 372,* 8–14. https://doi.org/10.1016/j.powtec.2020.05.102

Wang, Y., Zhou, L., Wu, Y., & Yang, Q. (2018). New simple correlation formula for the drag coefficient of calcareous sand particles of highly irregular shape. *Powder Technology, 326,* 379–392. https://doi.org/10.1016/j.powtec.2017.12.004

White, F. (2011). *Fluid Mechanics. 7th Edition*. McGraw-Hill.

Zhang, P., & Mohseni, K. (2019). Viscous drag force model for dynamic Wilhelmy plate experiments. *Physical Review Fluids*, *4*(8), 084004. https://doi.org/10.1103/PhysRevFluids.4.084004

Zhao, R., Zhou, Y., Zhang, D., & Gao, X. (2022). Numerical investigation of the hydraulic transport of coarse particles in a vertical pipe based on a fully-coupled numerical model. *International Journal of Multiphase Flow*, *155,* 104094. https://doi.org/10.1016/j.ijmultiphaseflow.2022.104094

Zhou, C., Su, J., Chen, H., & Shi, Z. (2022). Terminal velocity and drag coefficient models for disc-shaped particles based on the imaging experiment. *Powder Technology*, *398*, 117062. https://doi.org/10.1016/j.powtec.2021.117062